

Short Communication

Effects of Ti on Microstructure, Mechanical Properties and Corrosion Behavior of High-Strength Steel Weld Metals for Offshore Structures

Jianguo Chen^{1,2,3,*}, Yongmei Yang^{1,4,5}, Liqun Li³, Zejun Wang², Huiying Xiao^{1,4,5,*}, Yushun Wei², Tenghui Zhu^{1,4,5}, Hong Sun^{1,4,5}

¹ Tianjin Yongchang Welding Wire Co., Ltd., Tianjin 300300, PR China;

² Tianjin Special Equipment Inspection Institute, Tianjin 300192, PR China;

³ School of Materials Science and Engineering, Harbin Institute of Technology, Harbin 150001, PR China;

⁴ Tianjin key laboratory of high-end equipment manufacturing welding consumables and technology enterprises, Tianjin 300300, PR China;

⁵ Tianjin Golden Bridge Welding Materials Group Co., Ltd., Tianjin 300300, PR China;

*E-mail: jianguo_chen123@163.com (Jianguo Chen), xiao731120@163.com (Huiying Xiao)

Received: 18 April 2021/ Accepted: 6 June 2021 / Published: 30 June 2021

Micro-alloying elements significantly affect the microstructure, mechanical properties and corrosion behavior of the high-strength steel weld metals. In this paper, the effects of Ti content on the microstructure, mechanical properties and corrosion behavior of 690 MPa level high-strength steel shielded metal arc welding (SMAW) weld metal were studied. It is indicated that the grain refinement strengthening is the main strengthening mechanism for the weld metals. The microstructure, the formation of the oxide, the mechanical properties, and the corrosion resistance of the weld metal were remarkably affected by the addition of Ti. With the increase of Ti content, the grains of the weld metal were refined. Both the tensile strength and corrosion resistance were improved, while the impact property decreased. The Mn and Si oxides were covered more completely by the Ti oxides with the increase of the Ti content, forming Mn, Si, and Ti complex oxides, which resulted in the increase of the acicular ferrite. However, excessive addition (0.022 wt.%) of Ti led to the decrease of the acicular ferrite and the formation of lath bainite. The formation of lath bainite is the main reason for the deterioration of the impact property and corrosion resistance of the weld metal.

Keywords: Microstructure, Ti content, Weld metal, 690 MPa high-strength steel, Mechanical properties, Corrosion behavior

1. INTRODUCTION

With the expansion of energy exploration to the depths of the ocean, the extension for the offshore structures is an essential strategy. Aimed at reducing weight, ultra-high strength is the main

concern for the heavy-duty steel plates in the new generation of offshore structures. As an important structural material of offshore engineering equipment, high-strength steels are widely used in drilling platforms, work platforms, and subsea pipelines. Among them, the key components, such as the legs and cantilever beams of jack-up drilling platforms, require a large number of high-strength steels with the yield strength levels close to 690 MPa. Welding is regarded as the main installation and manufacturing technology of offshore engineering equipment, accounting for about 45% of the total manufacturing work. The quality of the high-strength steel welding directly determines the safety and reliability of the offshore equipment.

Stringent requirements are made on the strength and toughness of corresponding welding consumables for the use of high-strength steel [1]. Unfortunately, most of the existing welding consumables for high-strength steel have high yield ratio and poor plasticity, because it is very difficult to maintain high toughness in the case of high strength. Adding micro-alloying elements is a common method to adjust the weld metal structure and mechanical properties. Generally [2], the microstructure of C-Mn weld metal consists of acicular ferrite, allotriomorphic ferrite, Widmanstätten ferrite and other micro-phases, and its yield range is from 350 to 450 MPa. Some high-strength low-alloy weld metals, such as C-Mn weld metal with a small amount of micro-alloying elements, have similar microstructures to conventional C-Mn weld metal, while they have a higher yield strength, generally in the range from 500 to 700 MPa. If the micro-alloying elements contents are further increased, the microstructure of weld metal will be transformed into a mixed structure of acicular ferrite, bainite, and even martensite, and the yield strength is increased to the range from 690 to 1000 MPa. Yet the strength and toughness of metal materials have a trade-off relationship. The increase of strength will result in a decrease of toughness. It is generally accepted that acicular ferrite is one excellent microstructure for achieving the balance between strength and toughness of C-Mn weld metal [3-5]. Some studies indicated that non-metallic oxides have an important influence on the formation of acicular ferrite in high-strength steel weld metal [6-8]. However, Non-metallic oxides formed by different micro-alloying element contents can act as the nucleation particle of acicular ferrite. They may also be the nucleation of voids during ductile fracture and act as initiation sites for cleavage fracture cracks during brittle fracture [9]. Therefore, micro-alloying elements cannot be added into the weld metal blindly, and there should be a clear range for the content of the micro-alloying elements. In addition, considering the service environment (marine environment) of 690 MPa level high-strength steel, its corrosion resistance is another critical factor to be considered. Although some researches were carried out on the corrosion resistance of 690 MPa level high-strength steel in simulated marine environment up to now [10-12], the corrosion resistance of its weld metal was rarely investigated.

The aim of the present study was to develop the welding materials for shielded metal arc welding (SMAW) of 690 MPa level high-strength steel in the offshore structure field. Ti, one of the most important micro-alloying elements to form non-metallic oxides, was selected as the research variable. The evolution of internal microstructure, non-metallic oxides, mechanical properties, and corrosion behavior of 690 MPa level high-strength steel weld metals with different Ti contents were discussed. The obtained results can promote the development of offshore industry and offer a reference for future similar research.

2. MATERIALS AND EXPERIMENT METHODS

2.1 Preparation of weld metals and mechanical experiments

The experimental steel matrix is the 690 MPa level steel produced on an industrial scale for offshore structures, and its chemical compositions are shown in Table 1. The welding consumable is an independently developed electrode for welding 690 MPa level high-strength steel. The dimensions of the plates to be butt-welded are $300 \times 120 \times 20 \text{ mm}^3$, and the size of the pad plate is $300 \times 25 \times 12 \text{ mm}^3$. The groove angle is 45° , and the root clearance is 15 mm. In the welding test, welding current was in the range of 150-170 A, and the interpass temperature was controlled at 150°C . The chemical compositions of the weld metals are shown in Table 2. The mechanical properties of the weld metals were tested on a 600 kN universal testing machine and a 450 J pendulum impact tester. The size of gauge section for the tensile specimen is $\Phi 6 \times 30 \text{ mm}$, and the size of the Charpy-V-notch sample is $10 \times 10 \times 55 \text{ mm}^3$. Three impact samples prepared under an identical condition are used to evaluate the impact property of weld metals at -60°C . Schematic cross-section of the weld metal is shown in Fig. 1 to show the positions of the specimens for the tests of the microstructure and the mechanical properties.

Table 1. Chemical composition of experimental steel in wt.%

| C | Si | Mn | S | P | Cr | Ni | Mo | Fe |
|------|------|------|-------|-------|------|------|------|------|
| 0.06 | 0.25 | 1.37 | 0.004 | 0.008 | 0.40 | 2.44 | 0.35 | Bal. |

Table 2. Chemical compositions of weld metals in wt.%

| Weld metal | C | Si | Mn | S | P | Cr | Ni | Mo | O | Ti | Fe |
|----------------|-------|------|------|-------|-------|------|------|------|-------|-------|------|
| T ₁ | 0.038 | 0.22 | 1.44 | 0.006 | 0.006 | 0.36 | 2.58 | 0.45 | 0.089 | 0.001 | Bal. |
| T ₂ | 0.040 | 0.21 | 1.43 | 0.006 | 0.011 | 0.37 | 2.53 | 0.45 | 0.079 | 0.012 | Bal. |
| T ₃ | 0.042 | 0.28 | 1.56 | 0.006 | 0.006 | 0.38 | 2.44 | 0.44 | 0.071 | 0.018 | Bal. |
| T ₄ | 0.045 | 0.31 | 1.60 | 0.005 | 0.008 | 0.38 | 2.47 | 0.44 | 0.077 | 0.022 | Bal. |

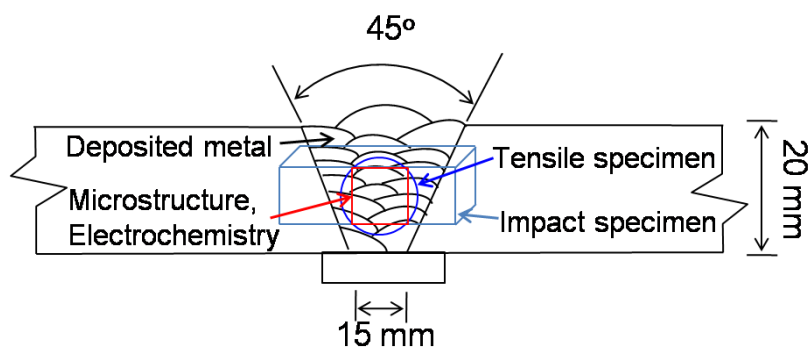


Figure 1. Schematic cross-section of microstructure and mechanical properties test specimens taken in weld metal.

2.2 Microstructure analysis

The metal blocks for microstructure examination were sanded using a series of SiC papers (400#, 600#, 800#, 1000#, 1500#, and 2000#) followed by polishing and cleaning. Subsequently, the specimens were etched in a 4% nitric acid alcohol solution. Finally, the corroded specimens were placed in alcohol for ultrasonic cleaning, and then dried. OLYMPUS DSX510 optical microscopy (OM) was used for metallographic observation of weld metals. In order to further explore the microstructure and non-metallic oxides evolution mechanism of the weld metal, as well as the morphological characteristics of the fractures, the metallographic specimens and fractures were observed using a ZEISS GeminiSEM500 scanning electron microscope (SEM) with energy dispersive spectrometer (EDS). The phase constitution and morphology of the corrosion products after the weld metals block immersion test were detected by X-ray diffractometer (XRD) and SEM.

2.3 Electrochemical corrosion

The electrochemical measurements of weld metals were performed using PARSTAT 4000A electrochemical workstation with the three-electrode system at room temperature. The superficial area of the specimens was 1cm^2 . The electrolyte was a saturated 3.5 wt.% NaCl solution. The three electrodes included a saturated calomel electrode as the reference electrode (RE), a platinum sheet as the counter electrode (CE) and the specimen as the working electrode (WE). The scanning rate for the potentiodynamic polarization (PP) curves was 0.5 mV/s .

3. RESULTS AND DISCUSSION

3.1 Microstructure of weld metals

3.1.1 OM and SEM of weld metals

Fig. 2 shows the OM images of the weld metals with different Ti contents. It can be seen that the T₁ weld metal (0.001 wt.% Ti) contains the coarsest grains. As the Ti content increases, the microstructure of the weld metal is significantly refined. The Ti oxides in the weld metal have a strong pinning effect to the grain boundaries, thereby refining the grain size [13]. In addition, the incorporation of Ti also changes the morphology of the microstructure in the weld metals.

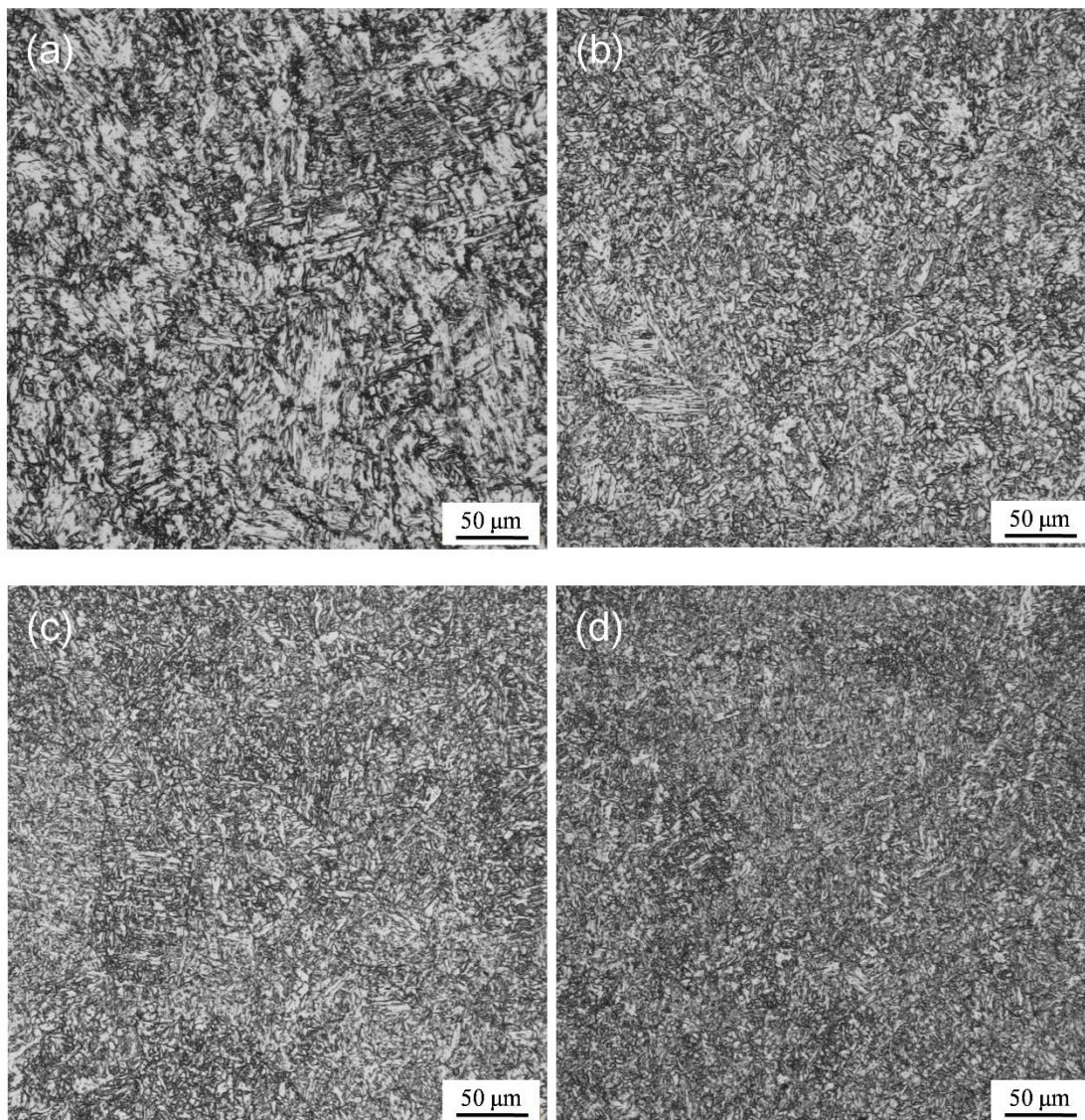


Figure 2. OM images of weld metals, (a) T₁ weld metal, (b) T₂ weld metal, (c) T₃ weld metal, and (d) T₄ weld metal.

In order to further analyze the microstructure evolution of the weld metals, Fig. 3 shows the SEM images of the weld metals with different Ti contents. The microstructure of T₁ weld metal (0.001 wt.% Ti) consists of granular bainite, polygonal ferrite, and a small amount of white bright-colored M-A islands. The granular bainite is relatively coarse and the polygonal ferrites distributed among the granular bainites. With the increase of the Ti content, the number of the polygonal ferrite and the granular bainite in the microstructure decreased considerably, and the content of the acicular ferrite in T₃ weld metal (0.018 wt.% Ti) is the largest. When the Ti content is further increased to 0.022 wt.%, the content of the acicular ferrite is reduced, and that of the lath bainite is increased. Moreover, part of the lath bainite is arranged in parallel, as shown in Fig. 3(d).

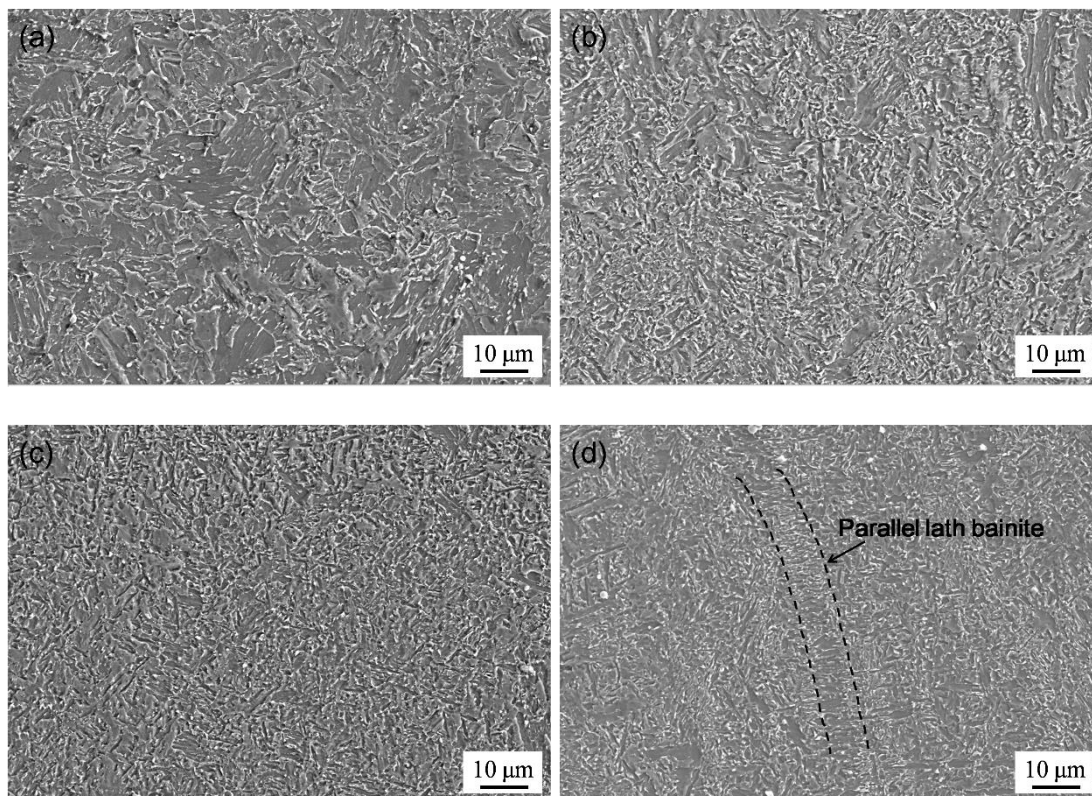


Figure 3. SEM images of weld metals, (a) T₁ weld metal, (b) T₂ weld metal, (c) T₃ weld metal, and (d) T₄ weld metal.

3.1.2 Acicular ferrite nucleation mechanism

Fig. 4 shows the SEM image of the non-metallic oxides in T₁ weld metal (0.001 wt.% Ti). The EDS mapping analyses showed that the non-metallic oxides mainly consist of Mn, Si, and O elements. The size of the non-metallic oxides is about 0.2 μm. Fattahi et al. claimed that the non-metallic oxides with a size about 0.2 μm have poor nucleation ability for acicular ferrite in weld metals [13]. The EDS mapping analyses of the non-metallic oxides in T₃ weld metal (0.018 wt.% Ti) indicated that the oxides are composed of Mn, Si, Ti, and O elements, as shown in Fig.5. The size of Mn, Si, and Ti complex oxides is determined to be about 0.8-1.2 μm, which is more favorable for the nucleation of the acicular ferrite [14]. The formation of Mn, Si, and Ti complex oxides can be inferred by comparing Fig. 5(a) and Fig. 5(b). In the early stage of Mn, Si, and Ti oxides formation, Ti oxides would first partially cover the Mn and Si oxide in the form of shell, as shown in Fig. 5(a). Then the Mn and Si oxide is completely coated by Ti oxide, forming Mn, Si, and Ti complex oxides, as shown in Fig.5(b). These complex oxides can be used as the effective nucleation position of acicular ferrite, since these oxides have good coherent relationship with the iron matrix [15]. In addition, Kang reported that a Mn depleted zone appeared near the non-metal oxide particle with the increase of Ti content in the high-strength low-alloy steel weld metal, which could facilitate the formation of the acicular ferrite [16].

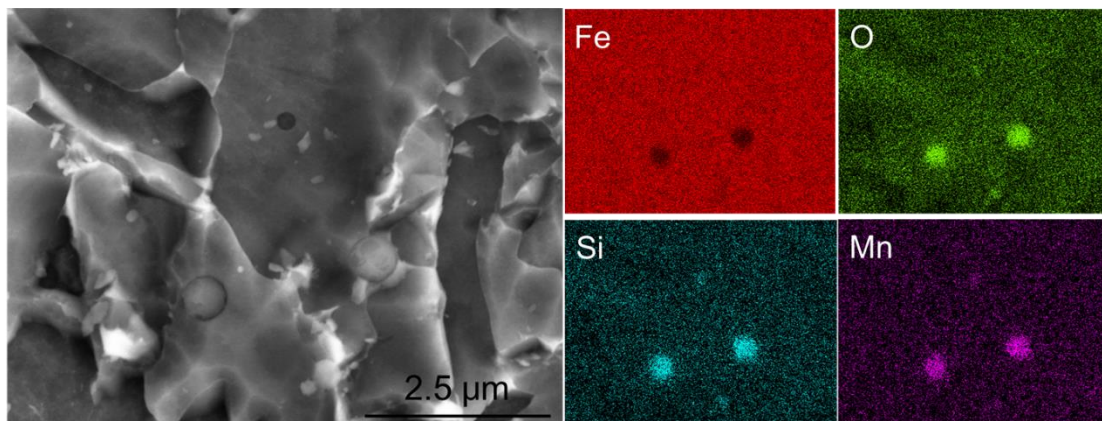


Figure 4. SEM and EDS mapping images of the oxide particles element distribution in T₁ weld metal (0.001 wt.% Ti).

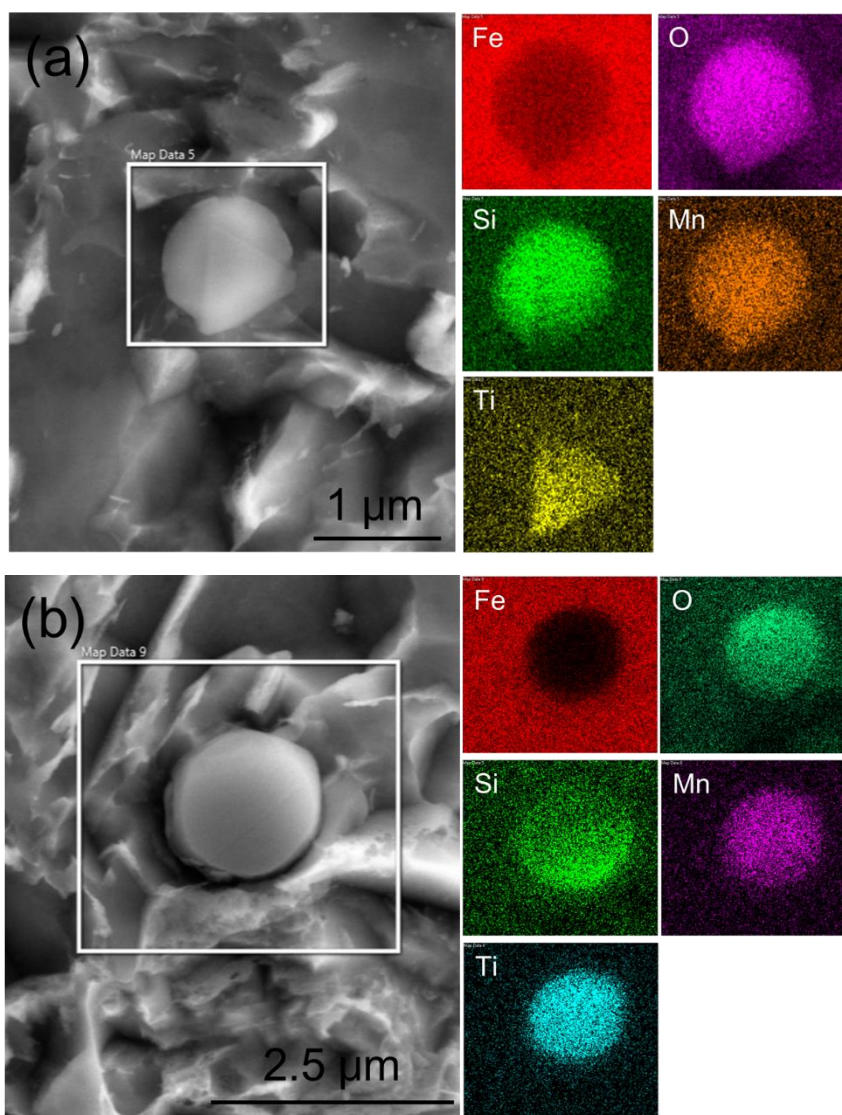


Figure 5. (a) and (b) SEM and EDS mapping images of the oxide particles element distribution in T₃ weld metal (0.018 wt.% Ti).

3.2 Mechanical properties of weld metals

3.2.1 Tensile properties of weld metals

Based on the regulations of the China Classification Society (CCS) [17], the yield strength (YS) of the weld metal of 690 MPa level steel is required to be 690 MPa or larger, and the ultimate tensile strength (UTS) should be in the range of 770-940 MPa. Fig. 6 shows the tensile properties of the weld metals with different Ti contents. Both the UTS and YS increase with the increasing Ti content. The UTS and YS of the other weld metals meet the CCS requirements except for the T₁ weld metal (0.001 wt.% Ti). Fig. 7 displays the tensile fracture morphology of weld metals. Numerous dimples are found in all the fractures, indicating a ductile fracture pattern. At the same time, the dimples gradually become shallower, and the fracture surface gradually flattens out from T₁ to T₄ weld metal, which corresponds to the change of tensile properties.

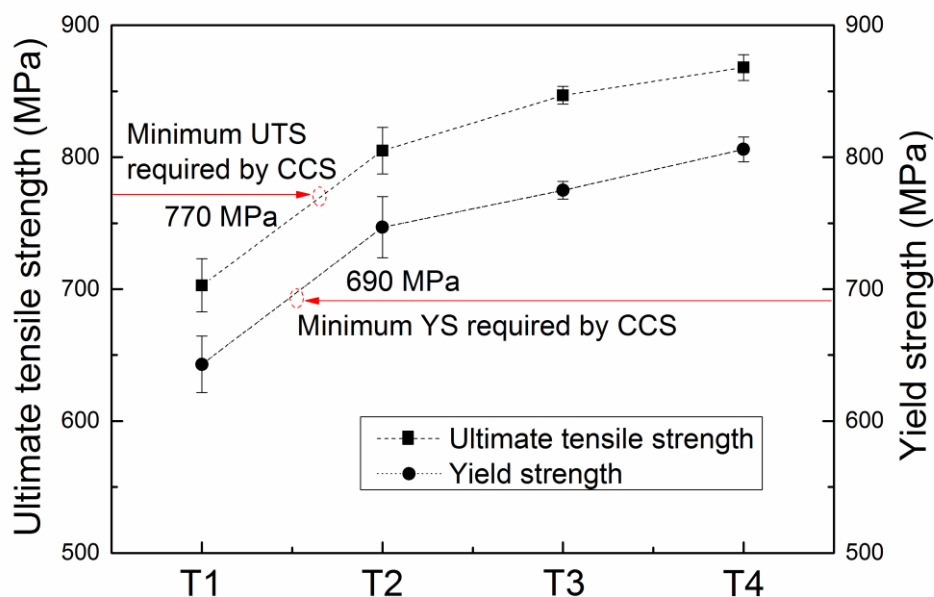
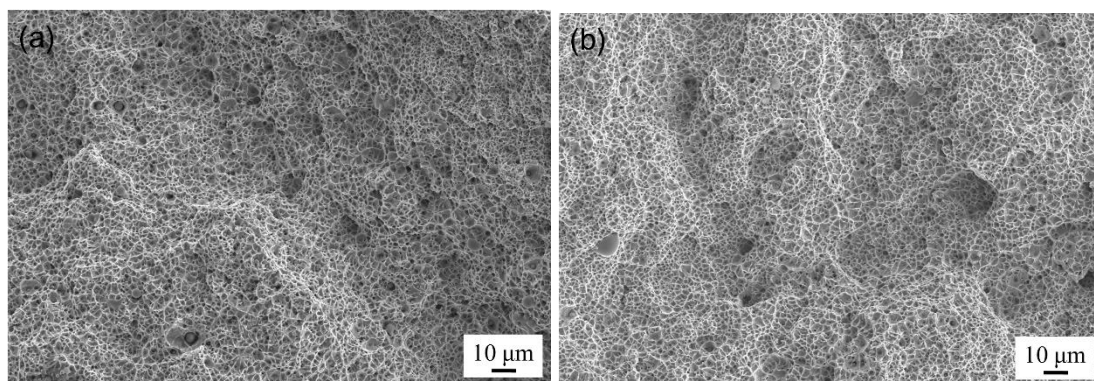


Figure 6. Tensile properties of weld metals with different Ti contents.



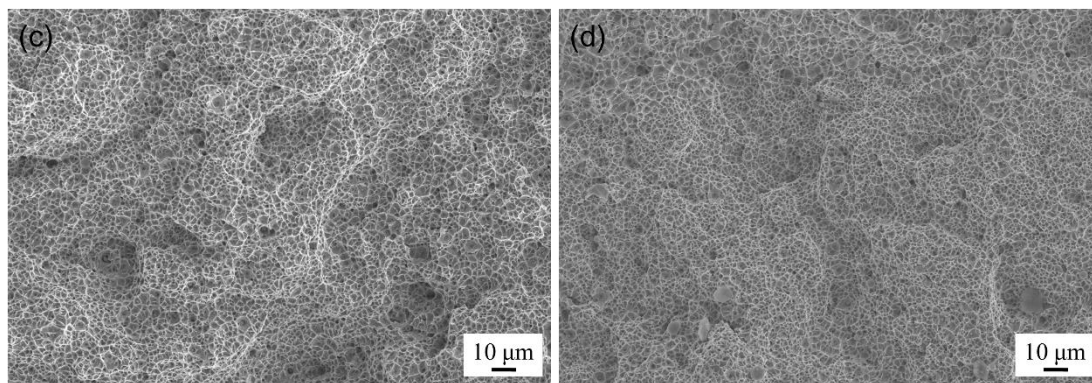


Figure 7. Tensile fractures of weld metals, (a) T₁ weld metal, (b) T₂ weld metal, (c) T₃ weld metal, and (d) T₄ weld metal.

3.2.2 Strengthening mechanism of weld metals

The strengthening effects of steel materials mainly include solution strengthening, fine grain strengthening, dislocation strengthening and dispersion strengthening. It is generally believed that the YS of the steel materials is equal to the sum of the above strengthening effects on the YS of material [18], namely:

$$\sigma_y = \sigma_0 + \sigma_{ss} + \sigma_{gb} + \sqrt{\sigma_{dis}^2 + \sigma_p^2} \quad (1)$$

where σ_y is the YS of the material, and σ_0 represents the frictional stress for the dislocation movement of pure iron, which is generally 54 MPa. σ_{ss} , σ_{gb} , σ_{dis} and σ_p are the contributions of solid solution strengthening, grain refinement strengthening, dislocation strengthening, and precipitation strengthening to the YS of the material, respectively.

The contribution of the solid solution strengthening to YS can be expressed as follows [19]:

$$\sigma_{ss} = \sum K_i \cdot C_i^z \quad (2)$$

where K_i is the correlation constant associated with the i -th alloy element, and C_i is the atomic percentage of the i -th alloy element. For the solid solution strengthening of the substituted atom, the value of Z is 0.75.

The contribution of the grain refinement strengthening to YS is given by the following equation [20]:

$$\sigma_{gb} = K_{gb} D^{-1/2} \quad (3)$$

where K_{gb} is a constant related to the material itself, and D is the grain size. As shown in Fig. 2, the grain size of the weld metal from T₁ to T₄ is decreasing. Therefore, the grain refinement strengthening effect of the weld metal from T₁ to T₄ is increasing.

The contribution of the dislocation strengthening and dispersion strengthening to YS can be expressed by the following equations, respectively [20,21]:

$$\sigma_{dis} = M \alpha G b \sqrt{\rho} \quad (4)$$

$$\sigma_p = 2Gb / L \quad (5)$$

where M is the Taylor factor ($= 3.06$), α is a constant ($= 0.38$), G is the shear modulus of iron

(=81.6 GPa), b is the Berkeley vector (= 0.25 nm), ρ is the dislocation density, and L is the average distance between dispersion strengthening phases.

The contribution of the solution strengthening, dislocation strengthening and dispersion strengthening to the YS of the weld metal in this study can be considered as follows. For solution strengthening, the chemical composition of the weld metal is almost the same, as shown in Table 2, so the solution strengthening effect is not the main reason for the difference in weld metal strength. As for the dislocation strengthening, in view of the fact that the processing and preparation processes of the weld metal are identical, therefore, the work hardening effect of the weld metal is not considered, while only the difference in the composition is considered. Among them, the C content has a direct effect on the dislocation density in the metal material, and the dislocation density increases linearly with the increase of the C content [22]. The chemical compositions of the weld metal in Table 2 show that the C content in the weld metal from T₁ to T₄ exhibits a slight increase trend (the difference is small), so the dislocation strengthening effect from T₁ to T₄ weld metal only shows a slight increase trend. The effect of the dispersion strengthening in this study can be ignored, which can be explained by the facts that the welding temperature is high and the cooling rate is fast. There is no chance for the precipitation of the nano-sized dispersion strengthening phases, and the non-metallic oxides for acicular ferrite nucleation in the weld metal is in large size and in little quantity. Therefore, they are not counted to be the dispersion strengthening phase in the strict sense.

According to the above discussion, it is concluded that the grain refinement strengthening plays a decisive role on the YS in this series of the weld metals. The grain refinement strengthening effect from T₁ to T₄ weld metal is increased, owing to the decrease of the grain size, as shown in Fig. 2. Especially, the grain refinement strengthening effect of the T₄ weld metal is the strongest, because its microstructure mainly contains lath bainite with the smallest grains, compared with other weld metals.

3.2.3 Impact toughness of weld metals

Low-temperature impact toughness is an important indicator for evaluating high-strength steel weld metal. CCS has clear requirements for the impact energy (IE) of 690 MPa level steel weld metal, i.e. the IE at -60 °C is not less than 69 J [17]. Fig. 8 shows the impact property of the weld metals with different content of Ti at -60 °C. It can be found that the impact property shows a downward trend with the increase of the Ti content. The impact property of the T₁ weld metal (0.001 wt.% Ti) is the highest. The ferrite and granular bainite in T₁ weld metal are plastic phases, so the T₁ weld metal has good toughness. As the Ti content increased, the content of the acicular ferrite was increased, as shown in the SEM images of T₂ and T₃ weld metals (Fig. 3). A large amount of acicular ferrite appeared in the T₃ weld metal (0.018 wt.% Ti). Acicular ferrite is a beneficial structure in high-strength steel weld metal, which can improve both the tensile and impact properties. Since the high-density grain boundaries in acicular ferrite can effectively prevent the cracks from propagating [23]. Therefore, the indexes for the mechanical properties of the T₂ and T₃ weld metals optimally meet the requirements of CCS, as shown in Fig. 6 and Fig. 8. It should be noted that the impact property is the lowest when the Ti content is increased to 0.022 wt.%. This may be related to the parallel lath bainite appeared in the microstructure,

as shown in Fig. 3(d). It was reported that this type of microstructure cannot effectively delay the crack growth [24].

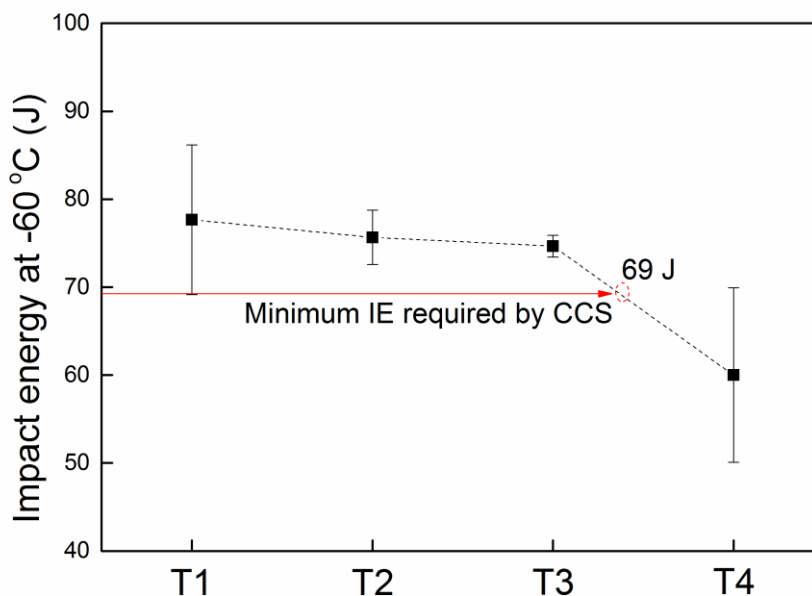
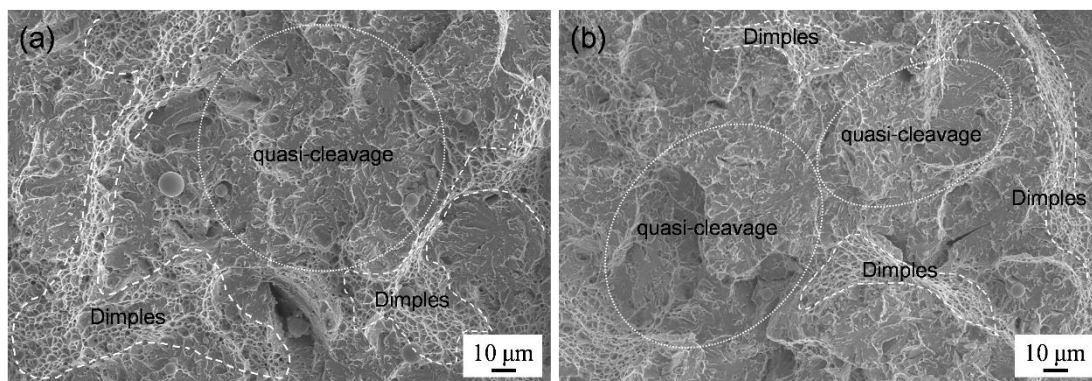


Figure 8. Impact property of weld metals with different Ti contents at -60 °C.

Fig. 9 shows the fracture morphology of weld metals after the -60 °C impact test. It can be found that the impact fractures from T₁ to T₃ weld metal consist of both dimples and quasi-cleavage facets, indicating a mixed pattern of ductile and brittle fracture. The dimples are mainly found at the top and lateral roots of the tearing ridge. With the increase of Ti, the fracture morphology of the weld metal changes significantly, and the proportion of dimples decreases, accompanied by the increase of the quasi-cleavage facets, as shown from Fig. 9(a) to (c). When the amount of Ti reaches 0.022 wt.%, the fracture is characterized by complete quasi-cleavage facets, and no trace of dimples is found, as shown in Fig. 9(d).



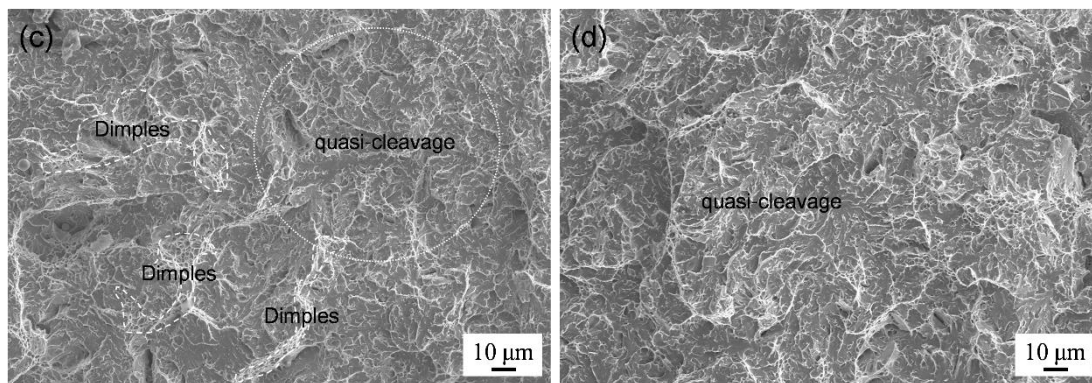


Figure 9. Impact fractures of weld metals at -60°C , (a) T_1 weld metal, (b) T_2 weld metal, (c) T_3 weld metal, and (d) T_4 weld metal.

3.3 Electrochemical corrosion property of weld metals

Through the previous analysis, it was found that the T_2 and T_3 weld metals meet the requirements of CCS. However, due to the sensitivity of steels used in the offshore structure field to corrosion, the corrosion resistance of the weld metals should also be studied. Fig. 10 shows the potentiodynamic polarization (PP) of weld metals as a function of Ti contents. The shapes of the PP curves are similar, revealing the similar corrosion mechanism for the weld metals in 3.5 wt.% NaCl solution. The current densities (i_{corr}) of each weld metal can be obtained from the Tafel extrapolation of both the cathodic and anodic branches of the polarization curves. The corrosion potentials (E_{corr}) and i_{corr} for the weld metals are listed in Table 3. It can be seen that the i_{corr} of the weld metal decreases first and then increases with the increase of the Ti content, and the change of the E_{corr} is opposite to the i_{corr} . Corrosion rate, the most direct parameters to evaluate the corrosion resistance of weld metals, can be expressed as follows [25]:

$$\text{Corrosion rate} = \frac{3.27 \times i_{\text{corr}} \times A}{nD} \quad (6)$$

where A is the atomic quantity, n is the number of electrons exchanged in the electrochemical reaction, and D is the density of the metals. For Fe-based materials [25], A can be regarded as the atomic quantity of iron ($= 55.84$), and D the density of iron ($= 7.90 \text{ g/cm}^3$), as well as the value of n is 2.

By comparing the values of the corrosion rate in Table 3, it can be found that the corrosion rate shows the same trend with the i_{corr} . Especially, the T_3 weld metal has the lowest corrosion rate, indicating that it has the strongest corrosion resistance.

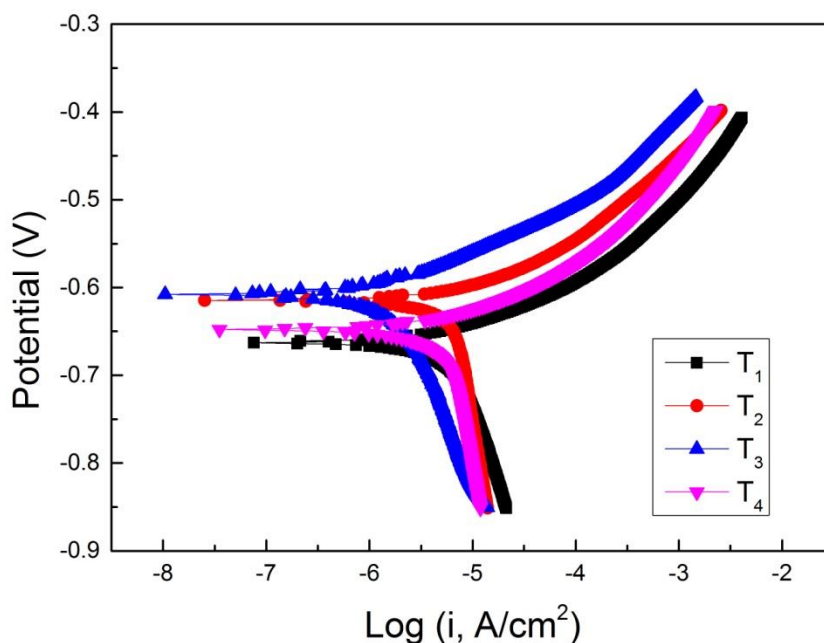


Figure 10. Potentiodynamic polarization curves of weld metals in 3.5 wt.% NaCl solution

Table 3. Electrochemical parameters of weld metals in 3.5 wt.% NaCl solution

| Weld metal | E_{corr} (V) | I_{corr} ($\mu\text{A}/\text{cm}^2$) | Corrosion rate ($\mu\text{m}/\text{y}$) |
|----------------|-----------------------|---|---|
| T ₁ | -0.663 | 3.76 | 43.45 |
| T ₂ | -0.615 | 3.19 | 36.87 |
| T ₃ | -0.607 | 2.12 | 24.50 |
| T ₄ | -0.648 | 3.52 | 40.68 |

The corrosion products of the weld metals corroded for 30 days in 3.5 wt.% NaCl solution were analyzed by XRD, as shown in Fig. 11. It can be found that there is no difference in the phase composition of the corrosion products. The rust layers were composed of iron oxyhydroxide, including α -FeOOH, β -FeOOH, and γ -FeOOH.

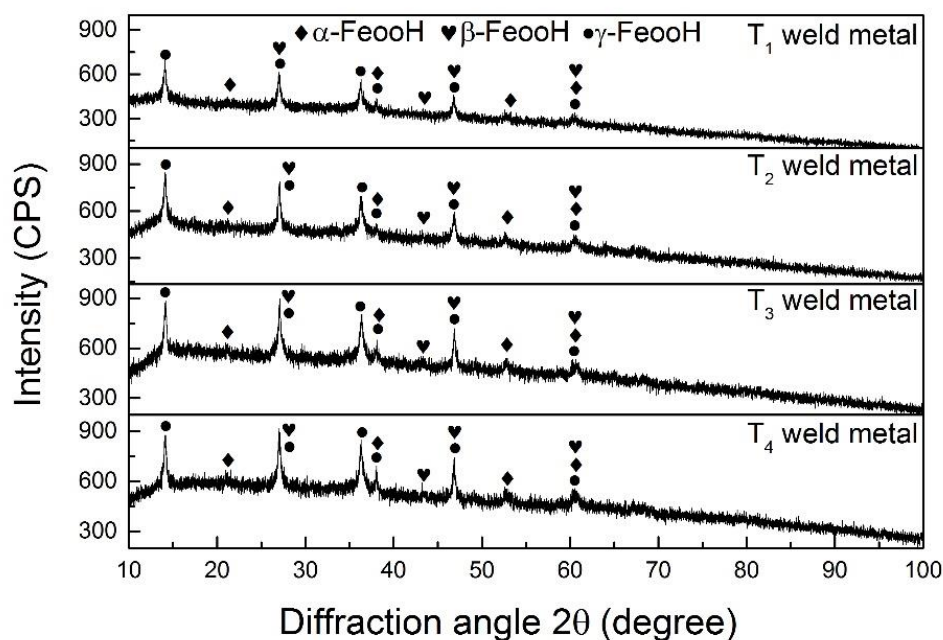


Figure 11. XRD phase analysis of corrosion products of weld metals corroded for 30 days in 3.5 wt.% NaCl solution

Fig. 12 shows the SEM micrographs for the cross sections of the weld metals after 30 days in 3.5 wt.% NaCl solution. It can be found that the thickness of the corrosion layer on the weld metal first decreases and then increases with the increasing Ti content, which is in good agreement with the electrochemical test results. The corrosion resistance is due to the difference in composition and microstructure of the weld metals. In this study, the corrosion resistance of the T₁ weld metal is the worst, because of the mixed microstructure of granular bainite, polygonal ferrite, and a small number of M-A islands. Previous work has shown that the M-A islands have a relatively higher Volta potential, compared with the ferrite matrix. The M-A islands can serve as cathodes in microgalvanic coupling, and accelerate the corrosion of adjacent substrates [26,27]. The corrosion resistance of the weld metals increases with the increase of Ti content from 0.001 to 0.018 wt.%. Ti could increase the pitting potential of the steel, and eliminate or reduce the grain boundary corrosion of the steel. As a result, the occurrence of pitting corrosion is suppressed, and the depth of the corrosion pit is further increased [28]. When the Ti content is increased to 0.022 wt.%, the corrosion resistance of weld metal decreases again. This can be explained by the fact that bainite phase, which contains many subgrain boundaries, has lower corrosion resistance than the ferrite phase [25].

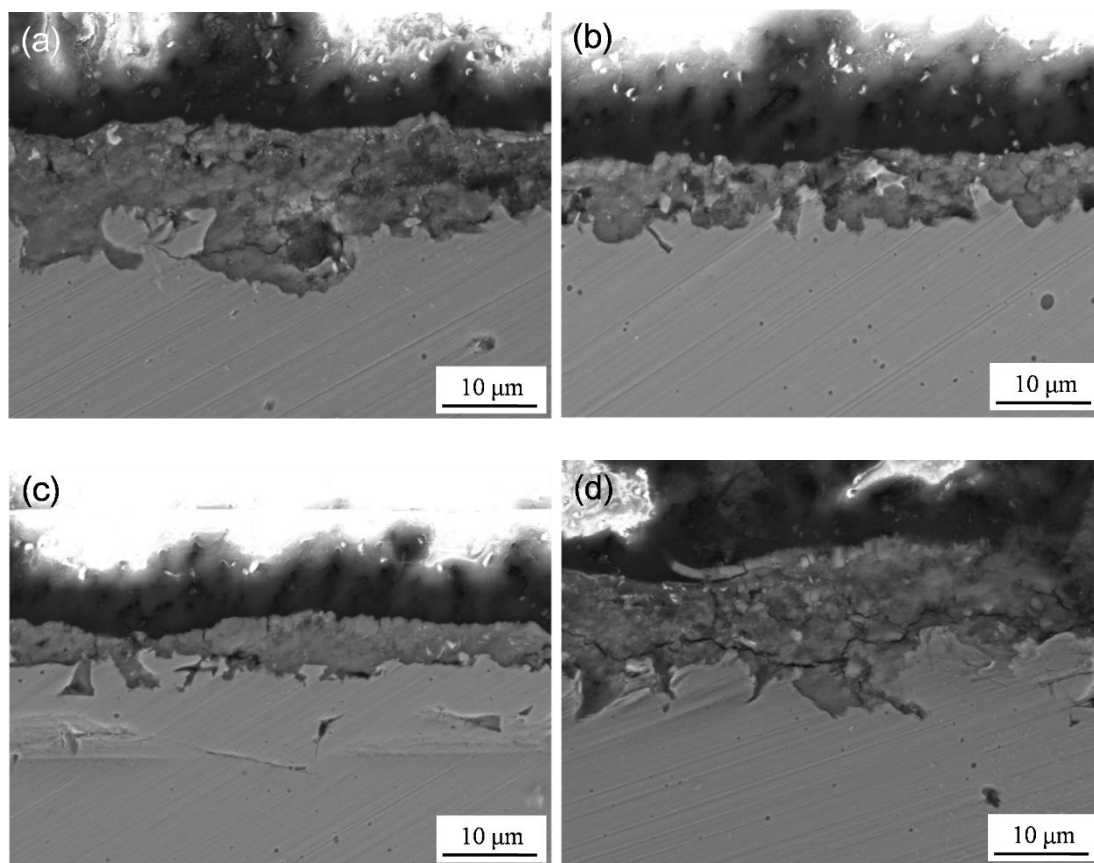


Figure 12. SEM micrographs of weld metals cross sections after 30 days in 3.5 wt.% NaCl solution, (a) T₁ weld metal, (b) T₂ weld metal, (c) T₃ weld metal, and (d) T₄ weld metal.

4. CONCLUSIONS

In this work, the effects of Ti on the microstructure, non-metallic oxides, mechanical properties, and corrosion behavior of 690 MPa level high-strength steel weld metals were discussed. The following conclusions can be drawn:

(1) There is almost no acicular ferrite in weld metal when the Ti content is 0.001 wt.%. The increase of the Ti content leads to the increase of the acicular ferrite in the weld metal. In the weld metal with 0.018 wt.% Ti addition, the acicular ferrite is the most. However, excessive addition (0.022 wt.%) of Ti results in the decrease of acicular ferrite in the microstructure.

(2) As the Ti content increases, Ti oxides cover on surface of the Mn and Si oxides, forming Mn, Si, and Ti complex oxides, which effectively accelerate the formation of acicular ferrite.

(3) Grains are obviously refined with the increase of Ti, and the grain refinement strengthening is the main strengthening mechanism for this series of weld metals.

(4) In this series of weld metals, the Ti addition amount has an optimal range (0.012 to 0.018 wt.%), under which the acicular ferrite appears in the microstructure, and the mechanical properties of the weld metals optimally meet the CCS requirements. When the Ti addition (0.001 wt.%) is lower than the optimal range, the tensile strength of the weld metal is low. When the Ti addition (0.022 wt.%) is higher than the optimal range, the low-temperature impact property of the weld metal is reduced.

(5) The corrosion resistance of the weld metal increases as the Ti content increases from 0.001 to 0.018 wt.%. When the Ti content was increased to 0.022 wt.%, the corrosion resistance of the weld metal deteriorates.

(6) Comprehensively considering the microstructure, mechanical properties, and corrosion resistance of the weld metal, it is believed that the T₃ weld metal with 0.018 wt.% Ti is most suitable for practical applications.

ACKNOWLEDGEMENTS

The work was financially supported by the Science and technology support key projects of Tianjin Key R&D Program (No. 20YFZCGX00150), and Science and Technology Program of Tianjin Administration for Market Regulation (No. 2019-W13 and 2018-W20).

References

1. T.L. Zhang, Z.X. Li, F. Young, H.J. Kim, H. Li, H.Y. Jing and W. Tillmann, *ISIJ Int.*, 54 (2014) 1472.
2. W.W. Bose-Filho, A.L.M. Carvalho and M. Strangwood, *Mater. Charact.*, 58 (2007) 29.
3. Y. Shao, C.X. Liu, Z.S. Yan, H.J. Li and Y.C. Liu, *J. Mater. Sci. Technol.*, 34 (2018) 737.
4. D.J. Abson, *Sci. technol. weld. joi.*, 23 (2018) 635.
5. C.X. Liu, L. Shi, Y.C. Liu, C. Li, H.J. Li and Q.Y. Guo, *J. Mater. sci.*, 51 (2016) 3555.
6. D.S. Sarma, A.V. Karasev and P.G. Jönsson, *ISIJ Int.*, 49 (2009) 1063.
7. D. Zhang, H. Terasaki and Y. Komizo, *Acta Mater.*, 58 (2010) 1369.
8. D. Loder, S.K. Michelic and C. Bernhard, *J. Mater. Sci. Res.*, 6 (2017) 24.
9. Q.L. Jiang, Y.J. Li, J. Wang and L. Zhang, *Mater. Sci. Technol.*, 27 (2011) 1565.
10. W. H. Huang, H.W. Yen and Y.L. Lee, *J. Mater. Res. Technol.*, 8 (2018) 1476.
11. W. Hao, Z. Liu, W. Wu, X. Li, C. Du and D. Zhang, *Mater. Sci. Eng. A*, 710 (2018) 318.
12. W. Wu, W.K. Hao, Z.Y. Liu, X.G. Li, C.W. Du and W.J. Liao, *J. Mater. Eng. perform.*, 24 (2015): 4636.
13. M. Fattahi, N. Nabhani, E. Rafiee, M. Nasibi, E. Ahmadi and Y. Fattahi, *Mater. Chem. Phys.*, 146 (2014) 105.
14. Z. Zhang, R.A. Farrar, *Mater. Sci. Technol.*, 12 (1996) 237.
15. B. Beidokhti, A.H. Koukabi and A. Dolati, *J. Mater. Process. Tech.*, 209 (2009) 4027.
16. Y. Kang, J. Jang, J.H. Park and C. Lee, *Met. Mater. Int.*, 20 (2014) 119.
17. China Classification Society, Rules for materials and welding, China Communications Press Co., Ltd., (2018) Beijing, China.
18. X.S. Zhou, Y.C. Liu, L.M. Yu, Z.Q. Ma, Q.Y. Guo, Y. Huang and H.J. Li, *Mater. Design*, 132 (2017) 158.
19. M. Dadé, J. Malaplate, J. Garnier, F. De Geuser, F. Barcelo, P. Wident and A. Deschamps, *Acta Mater.*, 127 (2017) 165.
20. Y. Shao, C.X. Liu, T.X. Yue, Y.C. Liu, Z.S. Yan and H.J. Li, *Mater. Sci. Eng. B*, 49 (2018) 1560.
21. J. Shen, Y. Li, F. Li, H. Yang, Z. Zhao, S. Kano, Y. Matsukawa, Y. Satoh and H. Abe, *Mater. Sci. Eng. A*, 673 (2016) 624.
22. S. Morito, J. Nishikawa and T. Maki, *ISIJ Int.*, 43 (2003) 1475.
23. Y.C. Liu, L. Shi, C.X. Liu, L.M. Yu, Z.S. Yan and H.J. Li, *Mater. Sci. Eng. A*, 675 (2016) 371.
24. Q.L. Jiang, Y.J. Li, J. Wang and L. Zhang, *Mater. Sci. Technol.*, 27 (2011) 1385.
25. D. Song, J. Hao, F. Yang, H. Chen, N. Liang, Y. Wu, J. Zhang, H. Ma, E.E. Klu, B. Gao, Y. Qiao, J. Sun and J. Jiang, *J. Alloy. Compd.*, 809 (2019) 151787.

26. H.C. Ma, J.B. Zhao, Y. Fan, Y.H. Huang, Z.Y. Liu, C.W. Du and X.G. Li, *Int. J. Fatigue*, 137 (2020) 105666.
27. H.C. Ma, Z.Y. Liu, C.W. Du, H.R. Wang, X.G. Li, D.W. Zhang and Z.Y. Cui, *Corros. Sci.*, 100 (2015) 627.
28. H. Wei, Y.L. Chen, W. Yu, L. Su, X. Wang and D. Tang, *Constr. Build. Mater.*, 239 (2020) 117815.

© 2021 The Authors. Published by ESG (www.electrochemsci.org). This article is an open access article distributed under the terms and conditions of the Creative Commons Attribution license (<http://creativecommons.org/licenses/by/4.0/>).